Published in final edited form as:
Comput Methods Appl Mech Eng. 2014 February 1; 269: 123–138. doi:10.1016/j.cma.2013.11.010.

A multiscale MD–FE model of diffusion in composite media with internal surface interaction based on numerical homogenization procedure

M. Kojic[a,b,*], **M. Milosevic**[b], **N. Kojic**[c], **K. Kim**[a], **M. Ferrari**[a], and **A. Ziemys**[a]

[a] Houston Methodist Research Institute, The Department of Nanomedicine, 6670 Bertner Ave., R7-116, Houston, TX 77030, USA

[b] Belgrade Metropolitan University, Bioengineering Research and Development Center BioIRC Kragujevac, Prvoslava Stojanovica 6, 3400 Kragujevac, Serbia

[c] Center for Engineering in Medicine and Surgical Services, Massachusetts General Hospital, Harvard Medical School, Boston, MA 02114, USA

Abstract

Mass transport by diffusion within composite materials may depend not only on internal microstructural geometry, but also on the chemical interactions between the transported substance and the material of the microstructure. Retrospectively, there is a gap in methods and theory to connect material microstructure properties with macroscale continuum diffusion characteristics. Here we present a new hierarchical multiscale model for diffusion within composite materials that couples material microstructural geometry and interactions between diffusing particles and the material matrix. This model, which bridges molecular dynamics (MD) and the finite element (FE) method, is employed to construct a continuum diffusion model based on a novel numerical homogenization procedure. The procedure is general and robust for evaluating constitutive material parameters of the continuum model. These parameters include the traditional bulk diffusion coefficients and, additionally, the distances from the solid surface accounting for surface interaction effects. We implemented our models to glucose diffusion through the following two geometrical/material configurations: tightly packed silica nanospheres, and a complex fibrous structure surrounding nanospheres. Then, rhodamine 6G diffusion analysis through an aga-rose gel network was performed, followed by a model validation using our experimental results. The microstructural model, numerical homogenization and continuum model offer a new platform for modeling and predicting mass diffusion through complex biological environment and within composite materials that are used in a wide range of applications, like drug delivery and nanoporous catalysts.

Keywords

Diffusion; Multiscale; Homogenization; Composite media; Finite element method; Molecular dynamics

[*] Corresponding author at: Houston Methodist Research Institute, The Department of Nanomedicine, 6670 Bertner Ave., R7-117, Houston, TX 77030, USA. Tel.: +1 713 441 7355; fax: +1 713 441 7438. mkojic42@gmail.com (M. Kojic)..

1. Introduction

Transport phenomena involving diffusion are commonly encountered in nature [1,2], in various technological processes [3,4] and biological systems [5,6], and thus have been thoroughly studied. Most of the research has focused on the macro-scale, where fundamental laws, such as Fick's or Darcy's law, describe movement of a given substance through a medium. Motion of solute particles through pores formed by complex microstructure may be affected not only by the solid pore boundaries, which dictate particle trajectories, but also by the physico-chemical interactions between the particles and solid surface occurring at the molecular level. The interactions between the diffusing substance and the surface become important and can profoundly affect overall diffusion when the spatial dimensions bounding diffusion are comparable to the diffusing particles or molecules [7,8]. Under these circumstances Fick's law alone cannot accurately describe diffusion and the surface interaction at the molecular level must be taken into account. Further in this study, we term Fickian diffusion as diffusion without surface interaction. The molecular dynamics (MD) technique enables the examination of diffusion with surface effects, where interactions at the atomistic and molecular level can be evaluated. Although MD is a widely employed and is extremely powerful tool, due to the exorbitantly large number of interactions needed to be considered, it can become impractical for even a small domain (on the order of micrometers). As technological breakthroughs, such as quantum computing, increase the computational power, it may one day become possible to perform large-scale MD simulations for practical applications. Until then, a computationally feasible method is needed to bridge the nano- and macroscale descriptions in order to model real-world complex diffusion processes.

In this study we present several new concepts. We first introduce a multiscale hierarchical model for diffusion at the microstructural level (further termed as ‘microstructural model’), within a small reference volume (RV). The implemented method is effective, robust, and generalizable to a variety of problems where diffusion governs transport. The method presented here can be easily expanded to include multiple molecule types (e.g. proteins, drugs), multiple surfaces (e.g. cells with different ligands/receptors, polymer fibers) and various media (different solvents). Further, we formulate a ‘continuum’ model which employs the results obtained by the microstructural model for diffusion within the RV. Our method relies on the fundamental condition of the equivalency of mass release kinetics between the continuum and microstructural models for a given region of space and over a prescribed concentration range. In formulating the continuum model, we introduce constitutive parameters, which include (traditional) equivalent ‘bulk’ diffusion coefficients (characterizing free, or Fickian, diffusion within the solvent), and also equivalent distances from an imaginary surface (describing surface effects within the microstructure [7]). Constitutive parameters, depending only on the structural geometry and the material properties of the diffusing constituents, are evaluated for three orthogonal coordinate directions – enabling modeling of general 3D diffusion conditions and anisotropy.

In order to construct the continuum model we introduce a novel numerical homogenization procedure. Previous homogenization procedures have limitations due to special assumptions made regarding microstructure (e.g. periodicity), as well as relying on various asymptotic expansions of analytic forms [9–13]. They have been extensively implemented in modeling diffusion within various porous media, [14–18], or in biological media [19–29]; however, these procedures are not readily generalizable. Our method is not only general (and overcomes the limitations of other homogenization procedures) but also includes concentration-dependent and new material parameters within a wide range of concentrations over which diffusion occurs. We demonstrate how to construct a model of diffusion through a composite material bounded by internal surfaces of arbitrary shape (e.g. representing tissue

fibers or the microstructure of an agarose gel), where the interactions between the molecules, medium, and internal surfaces considerably retard the diffusion kinetics compared to Fickian diffusion.

2. Basic hierarchical model

We here formulate the hierarchical diffusion model which is further used for introducing our homogenization procedure. Diffusion of particles or molecules through a porous medium represents motion of particles or molecules through fluid and is governed by the concentration gradient. Particle trajectories are affected by the pore and particle size and the overall diffusive properties can be considered dependent on porosity. This is realistic diffusion characterization for the case when the physico-chemical interactions between diffusing particles and solid surfaces of the microstructure can be neglected. However, in many cases, and particularly in diffusion of particles and molecules within biological media, the particle–surface interactions are very pronounced and strongly affect particle motion in the vicinity of the microstructural surfaces, modulating the diffusion process. These interaction effects are illustrated in Fig. 1a and b for diffusion within a nanochannel with a height *h* comparable to the particle size. Quantification of the surface interaction effects is performed using molecular dynamics (MD). This interaction is expressed as dependence of the effective diffusion coefficient on the distance from the solid surface and on the concentration, i.e. as $D(h,c)$, further used within finite element (FE) models. The methodology of coupling MD–FE models is described next.

2.1. MD simulations

Molecular dynamics (MD) has been used for several decades [30]. It is based on statistical mechanics, where motion of particles or molecules is described according to the Newtonian mechanics:

$$m_i\dot{\mathbf{v}}_i=\mathbf{F}_i \quad (1)$$

where m_i, $\dot{\mathbf{v}}_i$ and $\mathbf{F}_i$ aremass, acceleration and resulting force (including interaction forces fromthe neighboring particles and external forces), respectively. The interaction forces include bonded (repulsive-attractive, bending and torsion) and nonbonded (electrostatic, van der Waals) terms. The force field (FF) represents a functional form of behavior of chemical structures and is evaluated from potential energy function, $E = E_{inter} + E_{inter}$, of CHARMM FF [31] used in our MD models:

$$E_{intra}=\sum_{bonds} K_b(b-b_0)^2+\sum_{angles} K_\theta(\theta-\theta_0)^2+\sum_{torsions} K_\phi\,(1+\cos(n\phi+\delta)) \quad (2)$$

$$E_{inter}=\sum_{electrostatics}\frac{q_iq_j}{r_{ij}}+\sum_{VDW}\varepsilon_{ij}\left[\left(\frac{R_{\min,ij}}{r_{ij}}\right)^{12}+2\left(\frac{R_{\min,ij}}{r_{ij}}\right)^{6}\right] \quad (3)$$

Material parameters of the intramolecular potential E_{intra} are given by the force constants K_b;K_θ and K_φ, equilibrium values of bonds and angles b_0 and θ_0, and equilibrium torsion constants – dihedral multiplicity *n* and dihedral phase δ. Intermolecular potential sums are electrostatic and van der Waals (VDW) terms, where ε_{ij} is VDW potential depth, R_{min} is atom radius, and q_i; q_j are partial atomic charge. These parameters of FF are introduced to represent certain chemical classes of compounds in order to reproduce experimental physico-chemical properties.

MD simulations for calculating diffusivities in nanochannels were carried out [32,33] using NAMD 2.6 [34] with a TIP3P water model [35] and NVT (fixed number of particles N, volume V and temperature T) ensemble. CHARMM compatible amorphous silica force field [36] was employed to model the silica nanochannel, which is modeled by charged hydrophilic amorphous silica phase to match the silica properties after the fabrication process. Glucose diffusion coefficients were calculated from 30 ns trajectories by using the mean square displacement r^2:

$$\left\langle r^2 \right\rangle = 2dDt \quad (4)$$

where the factor d = 1–3 depends on the dimensionality of the space, and t is time. The diffusivity along the surface normal (y-direction) was evaluated, from the surface up to the middle of the nanochannel. The time window t for r^2 was chosen as 20 ps, which is small enough to catch local displacements within 0.5 nm thick slabs. Values of r^2 wereh collected to bins according to the center of mass of glucose molecules and their initial position. Glucose molecules could leave the bin in which r^2 is computed in order to avoid restricted ensemble. The diffusivity results include dependence on distance from the wall and glucose concentrations (Fig. 2a).

The MD calculated diffusivity is normalized with respect to the "bulk" value D_{bulk} corresponding to diffusivity far from the surface, where influence of the surface is negligible. Hence, we have

$$D = sD_{bulk} \quad (5)$$

where

$$s = s\left(h, c\right), \quad 0 \leq s \leq 1 \quad (6)$$

is the scaling function which depends on the distance from the wall surface h and concentration c. The calculated scaling functions for different concentrations are shown in Fig. 2b. Experimental investigations showed that $D(\equiv D_{bulk}$ for glucose depends on concentration, although data are quite different (see [7] and references given therein). For examples shown here we have chosen the glucose D according to the largest data set that spans over a wide range of concentrations, from 0 to 3.36 M [37].

The presented calculation of the effective diffusion coefficient and scaling function for the simple geometry of nanochannel can be extended to any microstructural construct. Namely, using MD we can determine diffusion coefficients $D_{\xi\xi}$, $D_{\eta\eta}$, $D_{\varsigma\varsigma}$ (or scaling functions s_ξ, s_η, s_ς) in the local system ξ, η, ς (Fig. 1c), where ξ is in the direction normal to the surface, and η, ς lie in the tangential plane:

$$\begin{aligned} D_{\xi\xi} &= s_\xi D_{bulk} \\ D_{\eta\eta} &= s_\eta D_{bulk} \\ D_{\zeta\zeta} &= s_\zeta D_{bulk} \end{aligned} \quad (7)$$

where D_{bulk} can depend on concentration, i.e. $D_{bulk} = D_{bulk}$ (c). Therefore, there are two domains in a microstructure: the domain with surface effects with the so-called hindered diffusion, and the bulk diffusion domain as shown in Fig. 1c. Diffusion tensor in the global coordinate system can be obtained by the tensorial transformation,

$$\mathbf{D} = \mathbf{T}\mathbf{D}_{\xi\eta\varsigma}\mathbf{T}^T \quad (8)$$

where $\mathbf{D}_{\xi\eta\zeta}$ is the diagonal tensor with components given in (7), while **T** is transformation matrix containing cosines of angles between local and global coordinate systems [38]. In the case of isotropic diffusion, the three scaling functions are equivalent $s_\xi = s_\eta = s_\zeta$ s(h, c) and the diffusion tensor is

$$\mathbf{D}=\mathbf{D}_{\xi\eta\varsigma}=s\,(h,c)\,D_{bulk}\mathbf{I} \quad (9)$$

where **I** is the identity tensor.

2.2. Finite element model

Finite element modeling of various problems in science and engineering has been well established [38–40]. We here consider unsteady diffusion where the diffusion coefficient depends on both concentration and spatial position of a point within the model. The fundamental constitutive relation is represented by the Fick's law,

$$\mathbf{J}--\mathbf{D}\nabla c \quad \text{or} \quad J_i=-D_{ij}\frac{\partial c}{\partial x_j} \quad (10)$$

where **J** is the mass flux, and summation on the repeated index is implied (j = 1–3).

FE solution procedures for nonlinear diffusion problems have been well established and successfully used in various applications [38–40]. The basic mass balance equation, which also includes Fick's law in Eq. (10), is

$$-\frac{\partial c}{\partial t}+\frac{\partial}{\partial x_i}\left(D_{ij}\frac{\partial c}{\partial x_j}\right)+q=0, \quad i,j=1-3 \quad (11)$$

where $c(x_i, t$ is concentration, and $q(x_i, t)$ is a source term. By using a standard Galerkin procedure, this nonlinear differential equation is further transformed into the incremental-iterative system of linear balance equations for a finite element [38]

$$\left(\frac{1}{\Delta t}\mathbf{M}+{}^{n+1}\mathbf{K}^{(i-1)}\right)\Delta\mathbf{C}^{(i)}={}^{n+1}\mathbf{Q}^{S(i-1)}+{}^{n+1}\mathbf{Q}^{V(i)}-{}^{n+1}\mathbf{K}^{(i-1)\,n+1}\mathbf{C}^{(i-1)}-\frac{1}{\Delta t}\mathbf{M}\left({}^{n+1}\mathbf{C}^{(i-1)}-{}^{n}\mathbf{C}\right) \quad (12)$$

where **C** is the vector of nodal concentrations; the left upper indices n and n + 1 denote values at the start and end of the time step n of size Δt; the indices i and i – 1 correspond to the current and previous equilibrium iteration, respectively; $\mathbf{Q}^S$ and $\mathbf{Q}^S$ and $\mathbf{Q}^V$ are surface and volumetric nodal fluxes for the element; and components of the matrices **M** and **K** are

$$M_{IJ}=\int_V N_I N_J dV \quad (13)$$

$${}^{n+1}K_{IJ}^{(i-1)}=\int_V {}^{n+1}D_{ij}^{(i-1)}N_{I,i}N_{J,j}dV \quad (14)$$

Here N_I and N_J are the interpolation functions, and ${}^{n+1}D_{ij}^{(i-1)}$ are components of the diffusion tensor corresponding to the last known concentration ^{n+1}c(i–1) at a point within the finite element, evaluated according to (7) and (8). Assembly of Eq. (12) and solution procedures are performed in a usual manner that is well described in the computational mechanics literature (e.g. [39]).

In our models we have incorporated concentration and interface effects, according to Eqs. (7) and (8). Implementation of the expression (7) is illustrated in Fig. 3. Note that linear interpolation between scaling curves is used.

The described hierarchical model has been verified by comparison of diffusion experiments in nanochannels [41]. Good agreement between computed and experimental results for mass release was found [7]. The effects of the surface interaction are shown in Section 4.1.

3. Numerical homogenization

Modeling of diffusion within a complex microstructure, with detailed evaluation of the field of diffusion tensor, requires significant effort in generating internal microstructural geometry and calculation of the scaling functions. This microstructural model is practically not applicable to compute diffusion in large domains, as for example, micron size domains in case of diffusion within biological tissues. Hence, a macroscale model with equivalent diffusion parameters is necessary for practical applications. We here introduce a new concept of numerical homogenization which relies on the described microstructural model, and also includes surface interaction between diffusing particles or molecules and solid surfaces during transport through fluid within pores of microstructure.

The basis for our homogenization procedure relies on the condition that mass release curves for the detailed microstructural and continuum models are the same (within a numerical tolerance). Namely, we select a small reference volume (RV) at a material point and calculate mass release curves for three coordinate directions; and then seek for equivalent diffusion parameters of the continuum to obtain the same mass release curves (see Fig. 4). If the equivalent parameters are determined under this condition, then the mass fluxes for the microstructural and continuum models

$$J_i=\frac{\partial m_i}{\partial t} \quad i=1-3 \quad (15)$$

are the same (graphical representation shown in Fig. 4) for any time during the diffusion process; here i = 1–3 stands for x, y, z. Therefore, diffusion characteristics will be the same for both models and the governing equation (11), which represents the mass balance equation:

$$-\frac{\partial c}{\partial t}-\frac{\partial J_i}{\partial x_i}+q=0 \quad i=1-3 \quad (16)$$

will yield the same solutions. Note that the microstructural model assumes MD calculation of the scaling functions for diffusing particles in microstructure and very fine FE mesh for discretization.

We introduce two sets of equivalent parameters:

- **a.** equivalent diffusion coefficients $\bar{D}_i$
- **b.** equivalent distances $\bar{h}_i$ from solid surfaces

for the three coordinate directions. The first set accounts for bulk diffusion within microstructure, and has been commonly used in the past in the homogenization procedures [16,42]. The new parameters $\bar{h}_i$ take into account surface interactions within the microstructure.

Practical evaluation of the equivalent parameters consists of the following steps:

1. Find mass release curves for the microstructural model with neglecting surface interaction effects within microstructure (Fickian diffusion);
2. Determine equivalent diffusion coefficients $\bar{D}_i$ using these mass release curves;
3. Evaluate scaling functions for the microstructure and determine mass release curves for the microstructural model using these scaling functions and the bulk diffusion coefficient D_{bulk};
4. Find equivalent distances $\bar{h}_i$ by employing mass release curves from step 3 and diffusion coefficients $\bar{l}_i$ from step 2.

These computational steps are illustrated in Fig. 5 for the case of linear dependence D_{bulk} (c). In calculating $\bar{D}_i$ we assume that the dependence $\bar{D}_i$ (c) is linear with the same slope (Fig. 5a) and search for the value $\bar{D}_i^0$ such that the mass release curves of the microstructural and continuum models are the same; the initial value of $\bar{D}_i^0$ is D_{bulk}^0. On the other hand, when searching for $\bar{h}_i$ we need to estimate the initial value $\bar{h}_i^0$. We briefly describe a way how we did this estimation. We discretize the RV space into a finite element mesh which is used for subsequent calculations. It is assumed that the microstructure consists of several material sets, and for each material set we calculate the scaling function for a representative concentration because diffusing particle may have different interaction with a different material (Fig. 5b). For illustration, a fibrous solid is assumed for the solid material set "s". We calculate for each point within the diffusion domain (e.g. point *P* in Fig. 5c) the distance h_s from the closest solid surface, using the appropriate local coordinate system (ξ, η, ζ in the figure). Then, we extrapolate the distance h_s to the FE nodes, by employing isoparametric functions [38,39], to obtain nodal values H_s^J (Fig. 5d). Further, we perform a weighting of these values according to the ratio of the total volume V_s of the set s with respect to the total volume of the solid phase V_{TOT}^s. Hence, the initial value $\bar{h}^0$ (for direction x_i) can be written as

$$\bar{h}_0 = \frac{1}{V_{TOT}^s} \sum_{s=1}^{N_s} V^s \bar{h}_s \quad (17)$$

where

$$\bar{h}_s = \frac{1}{N} \sum_{J=1}^{N} H_s^J \quad (18)$$

is the equivalent distance for the set *s*, and *N* is the number of nodes.

The mass release curves are generated by assuming that the entering surface is attached to a "reservoir" of volume V_{in} with initial concentration c_0, and that concentration at the opposite side is equal to zero; lateral surfaces are impermeable, ensuring one-directional diffusion conditions. The diffusion is calculated until concentration in RV and the inlet reservoir becomes close to zero, so that the mass release curve approaches a straight line parallel to the time-axis.

It is important to show that, for a given solvent and diffusing particles, equivalent diffusion parameters – equivalent diffusion coefficients and equivalent distances from surface – depend only on the geometry of the microstructure and its material characteristics. Then, it

can be stated that these are material parameters. We demonstrate the material character of the equivalent diffusion parameters in example in Section 4.4.

Finally, regarding the practical application of this multiscale model, we emphasize that RVs can be specified at various points of continuum and the equivalent diffusion parameters can be interpolated to capture variability of material properties within the macro-domain. Also, a sub-structuring concept may be applied to include some of RVs into the simultaneous calculations over time steps. The balance equations for RV coupled with continuum over common boundary nodes can be written as

$$\left(\hat{\mathbf{K}}_{bb} - \hat{\mathbf{K}}_{ba}\hat{\mathbf{K}}_{aa}^{-1}\hat{\mathbf{K}}_{ba}^{T}\right)\mathbf{C}_b = \mathbf{Q}_b = \hat{\mathbf{K}}_{ba}\hat{\mathbf{K}}_{aa}^{-1}\mathbf{Q}_a \quad (19)$$

where the indices *a* and *b* indicate internal and boundary nodes of RV matrices and nodal vectors, respectively.

4. Verification and application of multiscale models

In this section we first give a short overview of applicability and limitations of the introduced diffusion models, and then present numerical results to illustrate the main characteristics of the presented methodology which include both micro-structural and multiscale models. Also, the emphasis is on the surface interaction effects within microstructure on diffusion characteristics, which can be dominant and which have not been addressed in existing diffusion models. The examples include verification of the introduced methodology.

4.1. Notes about applicability of computational models

We here give general remarks about the complexity of the introduced models, their applicability and further generalizations.

It can be noted from the above model descriptions that the models are straightforward regarding computational methodology: (a) with a given microstructure geometry, physico-chemical properties of solvent, diffusing particles and micro-structural solid material, it is possible to compute scaling functions and evaluate mass release curves for the microstructural model; (b) it is then straightforward to numerically determine continuum diffusion parameters for all necessary microstructural models within the diffusion domain; and (c) solution of diffusion problem with given boundary and initial conditions, using the field of equivalent diffusive material parameters, reduces to a “standard” incremental-iterative steps. However, in some diffusion processes, such as those occurring within biological media (e.g. tissues or inter-cellular spaces) there is enormous complexity of the internal microstructure through which molecules or small particles are diffusing, as well as the inherent biological variability. Then, evaluation of scaling functions, as well as mass release curves of the microstructural models, represents a challenge and can be considered as limitations to practical medical applications. The obtained solutions include variability which is present in any biological process.

Regarding computational efficiency, it can be stated that a significant computational effort is required for MD calculations of effective diffusion coefficients for each microstructural material, and consequently scaling functions. Computation of mass release curves and equivalent diffusion parameters is very efficient since the FE models correspond to small regions, although the FE mesh must be very fine to properly capture the microstructural geometry; number of nodes (with concentration as one-degree of freedom) is measured by tens of thousands, and number of steps for mass release curves is on the order of thousands. For example shown in Fig. 11, we used a cube mesh 40 × 40 × 40 with 64,000 elements and

68,921 nodes. We run 40 time steps with different step duration for each of the cases with or without scaling functions. Evaluation of mass release curves and continuum parameters for each coordinate direction required 10 h of CPU using an Intel® Core™ i7-2600k processor. Size of continuum FE models depend on the size of the diffusion domain, but it can be handled easily with today's computers since the nodes are with one-degree of freedom.

Generally, the introduced models can serve as the basic models even for complex media, as is the case with micro-environments within living organisms. They can be further enhanced by introducing other processes occurring simultaneously with diffusion, such as, for example, matrix degradation. Even without further generalizations, the current models can be implemented to study transport of drugs in tissue, coupled with convective transport within capillary systems, in order to achieve more efficient therapies for tumor growth. We foresee that the described methodology can readily be applied in drug delivery, catalysis and other areas, where mass exchange is tightly coupled with microstructure of media.

4.2. Validation of the microstructural model

In this example we compute diffusion in a porous material, with microstructure composed of nanospheres as in Figs. 7a and 10c, using our microstructural model. These diffusion conditions correspond to those described in [16]. Calculation was performed by neglecting surface effects (Fickian diffusion) and for various porosities. Our results for the ratio of the effective diffusion coefficient D to the bulk value D_0, D/D_0, show very good agreement with values obtained by analytical homogenization procedure in [16]. Dependence D/D_0 on porosity φ was earlier obtained according to a self-consistent analytical method [42], and can be expressed in a simple form:

$$D/D_0 = \frac{2\phi}{3-\phi} \quad (20)$$

Results of this simple formula are displayed by dashed line in Fig. 6; deviation from our solution and in [42] becomes apparent for smaller porosities.

4.3. Effects of surface interactions in diffusion of glucose molecules (microstructural model)

We investigate diffusion characteristics of glucose molecules in water surrounded by a simple microstructure consisting of packed silica nanospheres for the cases when the spheres are separated by a small distance (Fig. 7a). The scaling functions correspond to glucose molecules and are shown in Fig. 7b [7]. Based on previous results [7,8], where good agreement between the numerical and experimental results was achieved, we here assume that the bulk diffusion coefficient linearly varies between 690 $\mu m^2/s$ for $c = 0$ and 267 $\mu m^2/s$ for $c = 2.75$ M. In order to model diffusion in the x-direction within the selected cubic RV, we assume that one side of the RV (“inlet” in Fig. 7a) is attached to a reservoir with initial concentration c_0, while the opposite side (“outlet”) is attached to a large-volume reservoir with a concentration $c = 0$..

Fig. 7c shows mass release curves for diffusion through the RV, for three different porosities, obtained for three values of sphere diameters (3, 6 and 8 nm). The minimum porosity corresponds to the special case when two neighboring spheres are touching. We assume that the scaling functions are the same for the normal and tangential directions, hence diffusion is isotropic in the entire domain. Mass release is hindered by surface interactions and these effects become more pronounced with decreasing porosities due to an

increase in the internal surface area (which results in a corresponding increase in the volume affected by surface interaction).

4.4. Demonstration that the equivalent diffusion parameters are material parameters

For a given solvent and diffusing particles we show that material parameters of the continuum model (equivalent diffusion coefficients and equivalent distances from surface) only depend on the geometry of the microstructure and its material characteristics. We take a reference volume (RV) containing solid silica nanospheres (as shown in Fig. 7a), with sphere diameters of 7 nm and porosity of 64%. For this model we change the boundary conditions to achieve various mass release curves.

Fig. 8 shows three mass release curves that differ significantly, obtained by changing inlet reservoir volume V_{in} for one order of magnitude (from 1.57 10^{-9} to 7.85 10^{-8} [μL]). Equivalent diffusion coefficient D and equivalent distance h are given in Table 1; they are practically the same for these mass release curves.

Another way to change mass release curves is to change initial concentration c_0. We have changed c_0 from 0.01 to 2.75 Molar, while keeping V_{in} unchanged. Mass release curves are shown in Fig. 9, while the calculated D and h are given in Table 2. Again, we see that the equivalent diffusion coefficient D and distance from surface h remain essentially unchanged.

Finally, we have doubled dimensions of the RV and calculated D and h. Table 3 demonstrates that these material parameters are independent of th RV size.

Data: 1. Model 1: cube side a_1 = 0:04 [μm], volume $V_{in}^1 = 7.850 \cdot 10^{-9}$ μl, number of spheres in RV is N_1 = 5 * 5* 5 125. 2. Model 2: = cube $a_2 = 2a_1$ = 0:08 [μm], volume $V_{in}^2 = 8V_{in}^1$, number of spheres is $N_2 = 8N_1$ = 10 * 10 * 10 = 1000.

4.5. Application of the multiscale continuum model

Here, we present several examples with simple and complex microstructures, which give insight into the multiscale continuum model formulation and the model applicability.

4.5.1. Microstructure with spheres and variable porosity—Fig. 10 shows mass release curves for the microstructural and continuum models, with a spherical solid internal structure and data as in Fig. 7a. Initial curves, for estimated (initial) parameters and the final curves (which overlap with the micro-structural solutions) are shown in Fig. 10a for porosity 0.64 (with and without surface effects). Agreement between micro-structural and continuum mass release curves in the presence of surface effects is depicted in Fig. 10b. We also examine cases where the microstructure consists of intersecting silica nanospheres (microstructure for 9% porosity is shown in Fig. 10c), and again we obtain continuum constitutive parameters such that mass release curves for the microstructural and continuum models are essentially identical (Fig. 10d). For this case of 9% porosity, the time needed for complete removal of the initial mass is now around 2.5×10^3 s which is three orders-of-magnitude greater than for larger porosities (Fig. 10b). The equivalent distance h increases from 0.52 nm to 2.05 nm, with an increase of porosity from 9% to 87%, respectively.

4.5.2. Diffusion of glucose molecules through complex microstructure—We consider diffusion of glucose molecules in water through a complex microstructure composed of fibers and spheres, which could represent a section of a biological tissue. The microstructure of this example is shown in Fig. 11c. For the selected internal geometry, the porosity is calculated to be 65%. The bulk diffusion coefficient (D_{bulk} = 690 $\mu m^2/s$) is assumed to be independent of concentration and the scaling functions are taken as in Fig. 7b.

The spatial distribution of the x-direction diffusion coefficient D_x at the first time step (t = 0.4 s) and at the RV boundary is shown in Fig. 11a, with the values ranging from zero (within and on the boundary of the solids) to 690 $\mu m^2/s$. Fig. 11b displays the spatial distribution of the mass flux in the x-direction J_x, having the same character of variation as D_x, while Fig. 11c shows distributions of J_x over several parallel planes. Mass release curves for the three coordinate directions (for both Fickian and with surface-influenced diffusion) are shown in Fig. 11d, and they are the same for the microstructural and continuum models. Values for the equivalent diffusion coefficients and equivalent distances are given in the figure legend. Based on these material parameters and the mass release curves, it is apparent that the continuum medium is anisotropic and that surface interactions significantly affect diffusion kinetics.

4.5.3. Diffusion of rhodamine 6G (R6G) molecules through an agarose polymer gel—Here, we first present detailed analysis of the microstructural model, and then compare the predictions of the equivalent continuum model with the experimentally obtained results. For the first task, we use the internal structure of the gel obtained by imaging [43], shown in Fig. 12a with discretized agarose fibers and porosity of 97%. As expected, the calculated diffusion in the x and y directions are roughly equivalent, since the size of the RV (0.934 × 0.934 μm) is large enough so that the overall characteristics are the same in the two directions. The bulk diffusion coefficient is D_{bulk} = 286 $\mu m^2/s$, while the scaling function, calculated using MD procedure, is displayed in the inset of Fig. 12b. To demonstrate that scaling functions may account for molecular size (zero diffusion in domain inside the radius of the molecule), two more scaling functions were created by off-setting the scaling function of R6G. Both microstructural and continuum models are used, giving the same total mass release. The release kinetics is slower for bigger molecules, since the scaling functions also incorporate the purely geometrical effects (size) of the diffusing molecules. The equivalent diffusion coefficients and equivalent distances from surface are given in the caption of Fig. 12.

In order to gain further insight into the diffusion within this polymer gel, we examine the mass flux and concentration distributions (Fig. 12c). Here, we consider the diffusion of molecules whose radius is 5 nm. The upper left panel shows the distribution of mass fluxes in the direction of diffusion at the end of the first time step, time t = 0.5 s. The field displays the variation of the flux due to the distribution of agarose fibers, with zero-values within the fibers and at the fiber surfaces. Diagrams of concentration and mass flux along the coordinate axes are shown in the lower-left and upper-right panels. Based on continuum solutions, the concentration decreases approximately linearly along line A–B, and remains constant along line C–D; flux-x is roughly constant along A–B, and flux-y is equal to zero along C–D. On the other hand, microstructural solutions have variations, with zero-values at the points corresponding to fibers. Finally, the right lower panel shows the solution for the concentration field obtained by the microstructural model at time t = 0.5 s; on average, concentration decreases along the x-axis, with zero-values at the fiber points. Taken together, the continuum model incorporates the microstructural flux fluctuations in order to achieve an equivalence of mass fluxes between the microstructural and continuum models through a given RV.

4.5.4. Verification example—For the multiscale model verification, we have experimentally measured R6G diffusion, where R6G was released from reservoirs into a sink through a 1% and 3% agarose hydrogel membrane. Mass release curves are calculated using the equivalent continuum model, based on the above microstructural model and the homogenization procedure. The equivalent diffusion coefficient and the equivalent distance from surface are given in the caption of Fig. 12 for R6G molecule with diameter of 0.3 nm. Fig. 13 shows experimental and computational curves normalized by the maximum released

mass M_∞, as $M(t)/M_\infty$. We use M_1 since our model does not include absorption which is also present in this mass transport. Simulated mass release curves in case of no surface interactions are practically the same for 1% and 3% due to the small difference in porosity, and show faster release than in case when surface effects are included. These effects are more pronounced for the 3% agarose hydrogel. However, our model captures both the porosity and surface effects within the microstructure, and shows good agreement with the experimental results, thus confirming the validity of our approach.

5. Summary and conclusions

We have formulated a microstructural hierarchical diffusion model for a general microstructural geometry, which includes interactions between the diffusing particles and the solid boundaries. In this model, the interaction effects are incorporated through scaling functions obtained from MD, which represent the ratios between the real and bulk diffusion coefficients. The scaling functions, expressed in terms of distance from the solid surfaces and concentration, are calculated in the local coordinate system of the solid surface. Therefore, two domains of diffusion are distinguished: the bulk diffusion domain (with Fickian diffusion) and the domain near surfaces, with non-Fickian hindered diffusion. In both domains, diffusion is calculated by using the FE method. The surface effects become apparent when comparing the slower mass release kinetics (with surface interactions) with purely Fickian mass release (without surface effects).

This microstructural model is then employed within a novel numerical homogenization procedure to establish the equivalent continuum diffusion model. The procedure is general since it is applicable to an internal structural geometry of any complexity, and can include different solid material sets with different material properties. The procedure relies on the condition that mass release curves of the two models must be equal. Constitutive diffusion parameters of the continuum model are determined for the three coordinate directions and include the traditional bulk diffusion coefficients, and also equivalent distances from the solid surfaces to account for surface interaction effects on diffusion. Furthermore, these constitutive parameters can depend on the local concentration. Our approach, consisting of a microstructural model and numerical homogenization procedure, is general and robust, and offers new possibilities in modeling diffusion through complex materials, including molecular transport in biological systems (e.g. intercellular spaces and tissues). The presented methodology has been experimentally validated and can serve as a tunable platform for constructing intricate multiscale hierarchical diffusion models with additional complexity and effects, such as multiple molecule types (e.g. different proteins/ligands), multiple surfaces (e.g. various cell types with different receptors), and various media (e.g. different solvents). These multiscale models provide a basis for a deeper, more accurate representation of fundamental transport processes occurring throughout nature.

Acknowledgments

The authors acknowledge the Texas Advanced Computing Center (TACC) at The University of Texas at Austin for providing HPC resources that have contributed to the research results reported within this paper. This project has been partially supported with Houston Methodist Research Institute, by the grants OI 174028 and III 41007 of the Serbian Ministry of Education and Science, and City of Kragujevac – Serbia. Authors also acknowledge partial supports from the following funding sources: the Ernest Cockrell Jr. Distinguished Endowed Chair (M.F.), US Department of Defense (W81XWH-09-1-0212) (M.F.), National Institute of Health (U54CA143837, U54CA151668) (M.F.).

References

1. Boving TB, Grathwohl P. Tracer diffusion coefficients in sedimentary rocks: correlation to porosity and hydraulic conductivity. J. Contam. Hydrol. 2001; 53:85–100. [PubMed: 11816996]

2. Zhang H, Selim HM. Second-order modeling of arsenite transport in soils. J. Contam. Hydrol. 2011; 126:121–129. [PubMed: 22115079]
3. Cao ZYH, Wang J, Tegenfeldt J, Austin R, Chen E, Wu W, Chou S. Fabrication of 10 nm enclosed nanofluidic channels. Appl. Phys. Lett. 2002; 81
4. Gardeniers H, Berg A. Micro-and nanofluidic devices for environmental and biomedical applications. Int. J. Environ. Anal. Chem. 2004; 84:809–819.
5. Desai TA, Hansford DJ, Kulinsky L, Nashat AH, Rasi G, Tu J, Wang Y, Zhang M, Ferrari M. Nanopore technology for biomedical applications. Biomed. Microdevices. 1999; 2:11–40.
6. Alber F, Dokudovskaya S, Veenhoff LM, Zhang W, Kipper J, Devos D, Suprapto A, Karni-Schmidt O, Williams R, Chait BT. Determining the architectures of macromolecular assemblies. Nature. 2007; 450:683–694. [PubMed: 18046405]
7. Ziemys A, Kojic M, Milosevic M, Kojic N, Hussain F, Ferrari M, Grattoni A. Hierarchical modeling of diffusive transport through nanochannels by coupling molecular dynamics with finite element method. J. Comput. Phys. 2011; 230:5722–5731.
8. Ziemys A, Kojic M, Milosevic M, Ferrari M. Interfacial effects on nanoconfined diffusive mass transport regimes. Phys. Rev. Lett. 2012; 108:236102–236105. [PubMed: 23003974]
9. Benssousan, JL.; Papanicoulau, G. Asymptotic Analysis for Periodic Structures. North-Holland; Amsterdam: 1978.
10. Ferrari M. Composite homogenization via the poly-inclusion approach. Compos. Eng. 1994; 4:37–45.
11. Hornung, U. Homogenization and Porous Media. Springer-Verlag; Berlin: 1997.
12. Nicolas MO, Oden JT, Vemagantia K, Remacle JF. Simplified methods and a posteriori error estimation for the homogenization of representative volume elements (RVE). Comput. Methods Appl. Mech. Eng. 1999; 176:265–278.
13. Allaire G, Pankratova I, Piatnitski A. Homogenization and concentration for a diffusion equation with large convection in a bounded domain. J. Funct. Anal. 2012; 262:300–330.
14. Sangani AS. An application of an homogenization method to a model of diffusion in glassy polymers. J. Polym. Sci. Part B Polym. Phys. 1986; 24:563–575.
15. Auriault JL, Lewandowska J. Effective diffusion coefficient: from homogenization to experiment. Transp. Porous Media. 1997; 27:205–223.
16. Boutin C, Geindreau C. Periodic homogenization and consistent estimates of transport parameters through sphere and polyhedron packings in the whole porosity range. Phys. Rev. E. 2010; 82(036313):036311–036318.
17. Vassal J-P, Orgéas L, Favier D, Auriault J-L. Phys. Rev. E. 2008; 77(011303):011301–011313.
18. Eitelberger J, Hofstetter K. Prediction of transport properties of wood below the fiber saturation point – a multiscale homogenization approach and its experimental validation. Part II: steady state moisture diffusion coefficient. Compos. Sci. Technol. 2011; 71:145–151.
19. Chen KC, Nicholson C. Changes in brain cell shape create residual extracellular space volume and explain tortuosity behavior during osmotic challenge. PNAS. 2000; 97:8306–8311. [PubMed: 10890922]
20. Rohan E. Modeling large-deformation-induced microflow in soft biological tissues. Theor. Comput. Fluid Dyn. 2006; 20:251–276.
21. Shorten PR, Sneyd J. A mathematical analysis of obstructed diffusion within skeletal muscle. Biophys. J. 2009; 96:4764–4778. [PubMed: 19527637]
22. Chapman SJ, Shipley RJ, Jawad R. Multiscale modeling of fluid transport in tumors. Bull. Math. Biol. 2008; 70:2334–2357. [PubMed: 18818972]
23. Chen Y, Zhou S, Li Q. Microstructure design of biodegradable scaffold and its effect on tissue regeneration. Biomaterials. 2011; 32:5003–5014. [PubMed: 21529933]
24. Sanz-Herrera JA, Garcia-Aznar JM, Doblare M. A mathematical model for bone tissue regeneration inside a specific type of scaffold. Biomech. Model. Mechanobiol. 2008; 7:355–366. [PubMed: 17530310]
25. Higgins ER, Goel P, Puglisi JL, Bers DM, Cannell M, Sneyd J. Modelling calcium microdomains using homogenisation. J. Theor. Biol. 2007; 247:623–644. [PubMed: 17499276]

26. Novak IL, Kraikivski P, Slepchenko BM. Diffusion in cytoplasm: effects of excluded volume due to internal membranes and cytoskeletal structures. Biophys. J. 2009; 97:758–767. [PubMed: 19651034]
27. Muha I, Naegel A, Stichel S, Grillo A, Heisig M, Wittum G. Effective diffusivity in membranes with tetrakaidekahedral cells and implications for the permeability of human stratum corneum. J. Membr. Sci. 2011; 368:18–25.
28. Rim JE, Pinsky PM, Osdol W.W.v. Using the method of homogenization to calculate the effective diffusivity of the stratum corneum with permeable corneocytes. J. Biomech. 2008; 41:788–796. [PubMed: 18093598]
29. Marciniak-Czochra A, Ptashnyk M. Derivation of a macroscopic receptor-based model using homogenization techniques. SIAM J. Math. Anal. 2008; 40:215–237.
30. Rapaport, DC. The Art of Molecular Dynamics Simulation. Cambridge University Press; 2004.
31. MacKerell A, et al. All-atom empirical potential for molecular modeling and dynamics studies of proteins. J. Phys. Chem. B. 1998; 102:3586–3616.
32. Ziemys A, Ferrari M, Cavasotto CN. Molecular modeling of glucose diffusivity in silica nanochannels. J. Nanosci. Nanotechnol. 2009; 9:6349–6359. [PubMed: 19908533]
33. Ziemys A, et al. Confinement effects on monosaccharide transport in nanochannels. J. Phys. Chem. B. 2010:132–137. [PubMed: 21155552]
34. Phillips JC, et al. Scalable molecular dynamics with NAMD. J. Comput. Chem. 2005; 26:1781–1802. [PubMed: 16222654]
35. Jorgensen WL, et al. Comparison of simple potential functions for simulating liquid water. J. Chem. Phys. 1983; 79:926–935.
36. Chu-Cruz ER, Aksimentiev A, Schulten K. Water silica force field for simulating nanodevices. J. Phys. Chem. B. 2006; 110:21497–21508. [PubMed: 17064100]
37. Gladden JK, Dole M. Diffusion in supersaturated solution II: glucose solutions. J. Am. Chem. Soc. 1953; 75:3900–3904.
38. Kojic, M.; Filipovic, N.; Stojanovic, B.; Kojic, N. Computer Modeling in Bioengineering – Theoretical Background, Examples and Software. John Wiley and Sons; Chichester, England: 2008.
39. Bathe, KJ. Finite Element Procedures. Prentice-Hall; Englewood Cliffs, N.J., USA: 1996.
40. Hughes, TJR. The Finite Element Method: Linear Static and Dynamic Finite Element Analysis. New York: 2000.
41. Fine D, Grattoni A, Hosali S, Ziemys A, Rosa ED, Gill J, Medema R, Hudson L, Kojic M, Milosevic M, Ferrari M. A robust nanofluidic membrane with tunable zero-order release for implantable dose specific drug delivery. Lab Chip. 2010; 10:3074–3083. [PubMed: 20697650]
42. Hashin Z. Assessment of the self consistent scheme approximation: conductivity of particulate composites. J. Compos. Mater. 1968; 2:284–300.
43. Griess GA, Guiseley KB, Serwer P. The relationship of agarose gel structure to the sieving of spheres during agarose gel electrophoresis. Biophys. J . 1993; 65:138–148. [PubMed: 8369423]

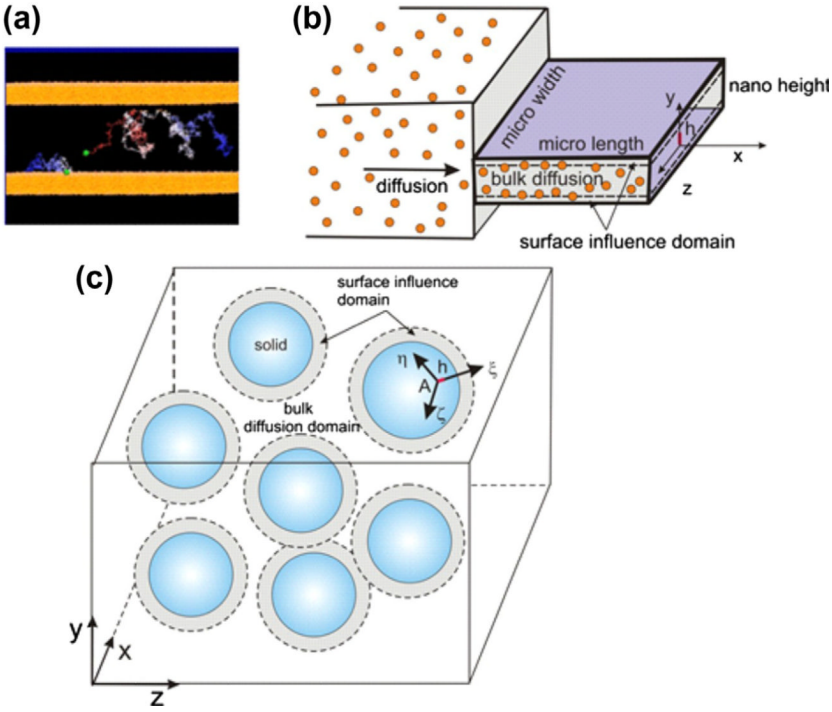

Fig. 1.

Diffusion within confined space. (a) Schematic of trajectories of molecules during diffusion within a nanochannel; (b) Bulk domain and domain of diffusion affected by interaction with surface in case of nanochannel of (nano) height *h*; (c) Bulk domain and surface influence domain in case of diffusion within a porous medium.

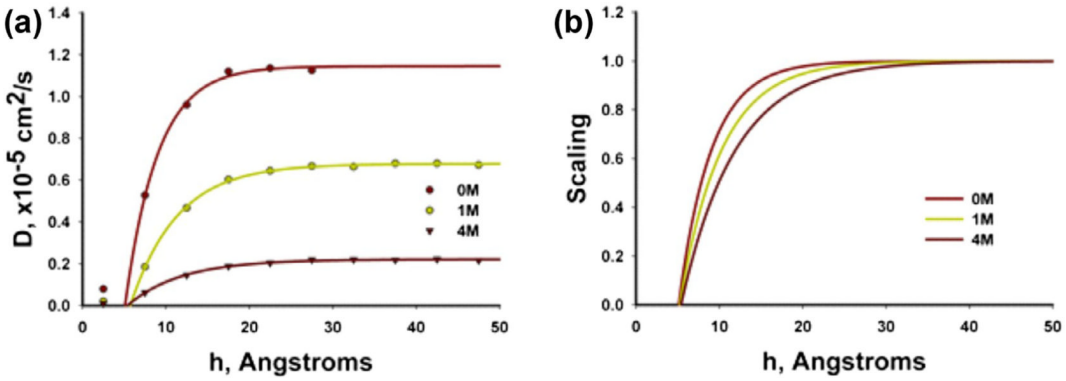

Fig. 2.

Diffusion scaling function of glucose calculated from MD as in [7]. (a) Glucose diffusion coefficient as a function of distance from silica surface for different glucose concnetrations. (b) Diffusion scaling functions, with the segment of zero diffusivity corresponding to statistical molecular radius.

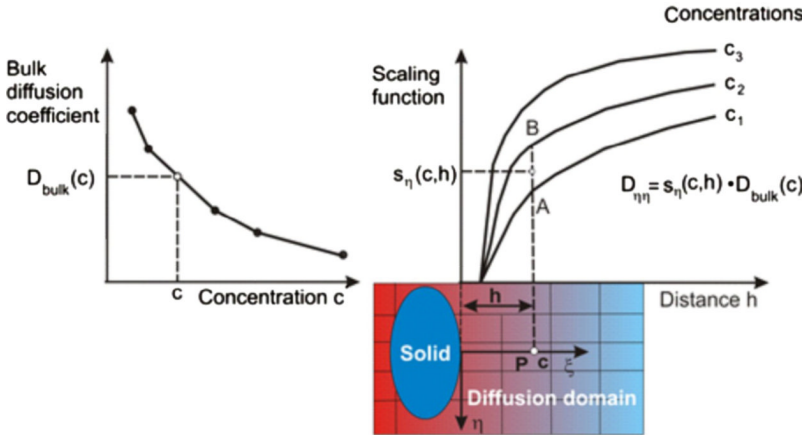

Fig. 3.

Determination of diffusion coefficient $D_{\eta\eta}$ at a spatial point *P* using dependence on concentration and surface effects. The "bulk" value is first determined from the curve $D_{bulk}(c)$; then, the scaling function is evaluated from a family of curves, with linear interpolation between curves $s(c,h)$ (between points *A* and *B* in the figure).

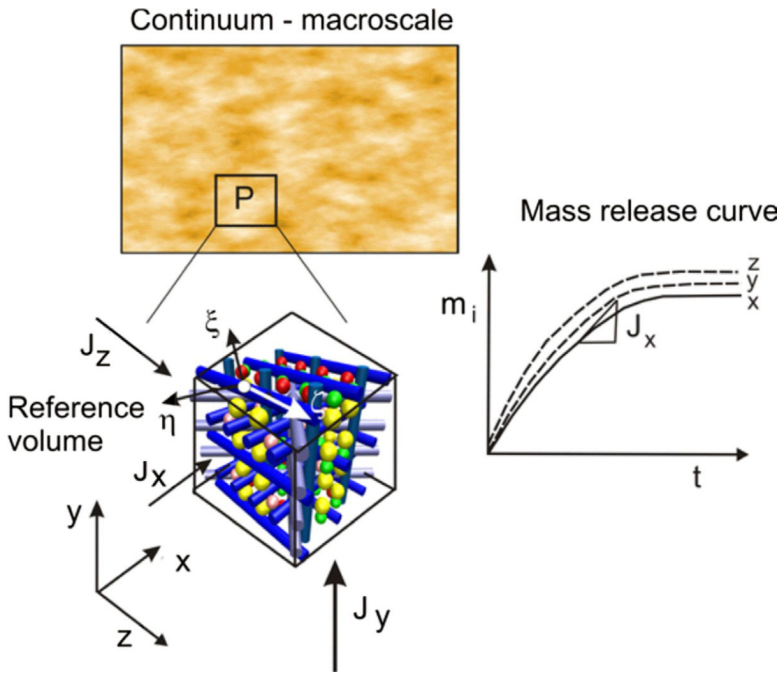

Fig. 4.

Illustration of the basic concept of numerical homogenization. A small reference volume (RV) is selected at point *P* of the medium and mass release curves $m_i(t)$ are evaluated by modeling diffusion in the coordinate directions *x*, *y*, *z* (i = 1–3). The microstructural model for diffusion within the RV contains a detailed description of the microstructure and the spatial field of the diffusion tensor is calculated using MD.

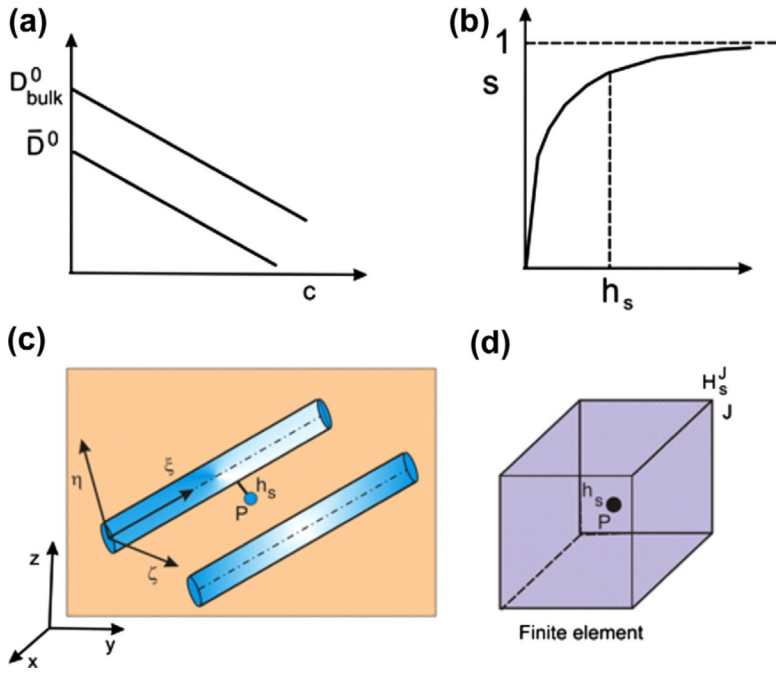

Fig. 5.

Details used in estimation of initial values. (a) Initial value $\bar{D}^{0}_{initial}=D_{bulk}$ and final value $\bar{D^{0}}$; (b) Scaling function for material set *s*; (c) Fibrous material set *s* with local and global coordinate systems; (d) Position of material point *P* within a finite element with distance h_s from surface and nodal value H_s^J at a node *J*.

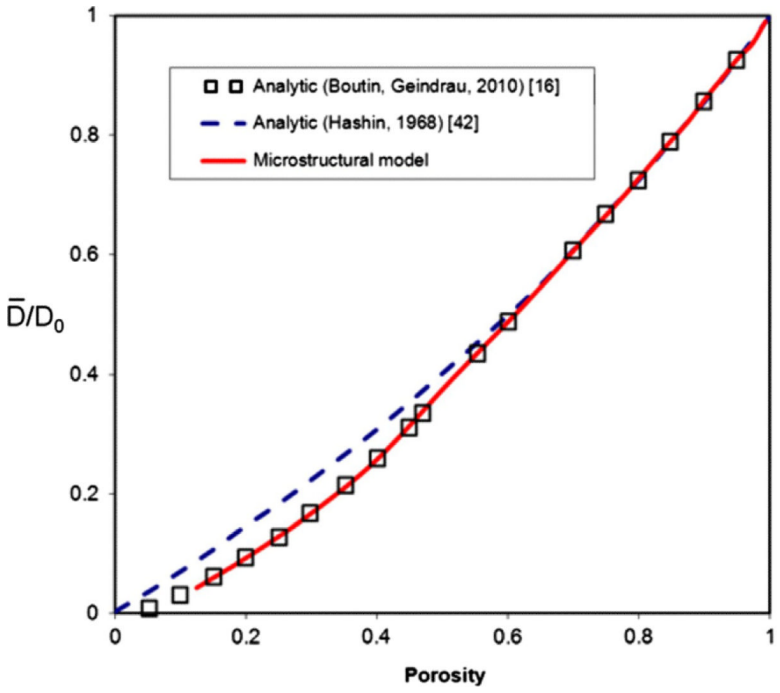

Fig. 6.

Ratio of the effective diffusion coefficient $\bar{D}$ with respect to the bulk value D_0; in terms of porosity. Our microstructural structure consists of spheres displaced as in Figs. 7a and 10c. Surface interaction is neglected, hence Fickian diffusion is assumed. Two analytical solutions are shown, according to Refs. [16,42].

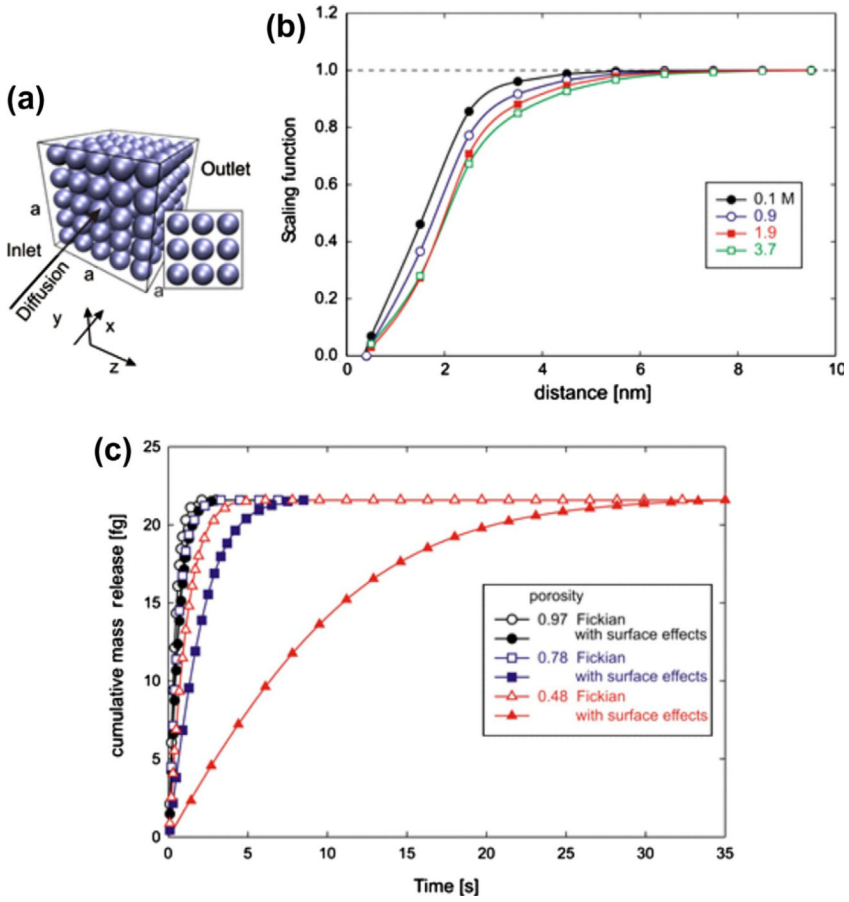

Fig. 7.

Diffusion through a porous medium consisting of packed silica nanospheres, microstructural model. (a) Internal structure of the medium; diffusion occurs from the inlet surface (attached to a reservoir with a prescribed volume and initial concentration c_0) to the outlet with concentration $c = 0$. Porosity is 0.78; (b) Scaling functions used in the analysis, according to [7], for diffusion through water of glucose molecules and silica surfaces; (c) Mass release curves for Fickian diffusion (no surface effects) and diffusion with surface effects, for three different porosities; minimum porosity 0.48 corresponds to the case when the spheres are just touching. Surface effects are more pronounced for smaller porosities due to a relatively larger internal surface.

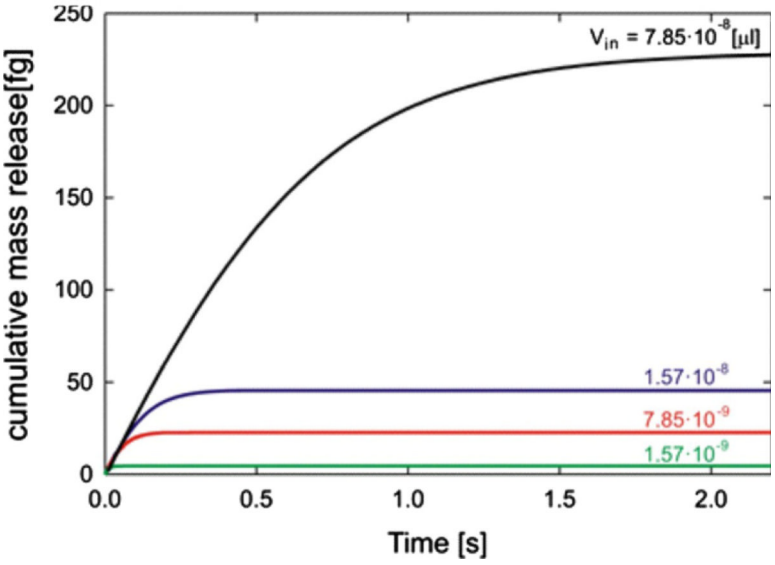

Fig. 8.

Mass release curves for volumes of the inlet reservoir from Table 1: 7.85 10^{-8}, 1.57 10^{-8}, 7.85 10^{-9} and 1.57 10^{-9} [μL].

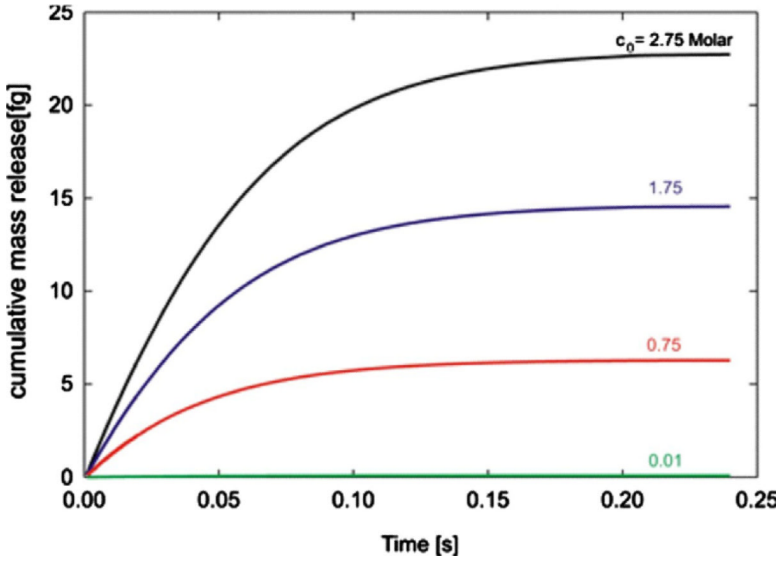

Fig. 9.

Mass release curves obtained for inlet reservoir volume $V_{in} = 7{:}850 \cdot 10^{-9}\mu L$ and four initial concentrations of the inlet reservoir c_0 (Molar): 2.75, 1.75, 0.75 and 0.01.

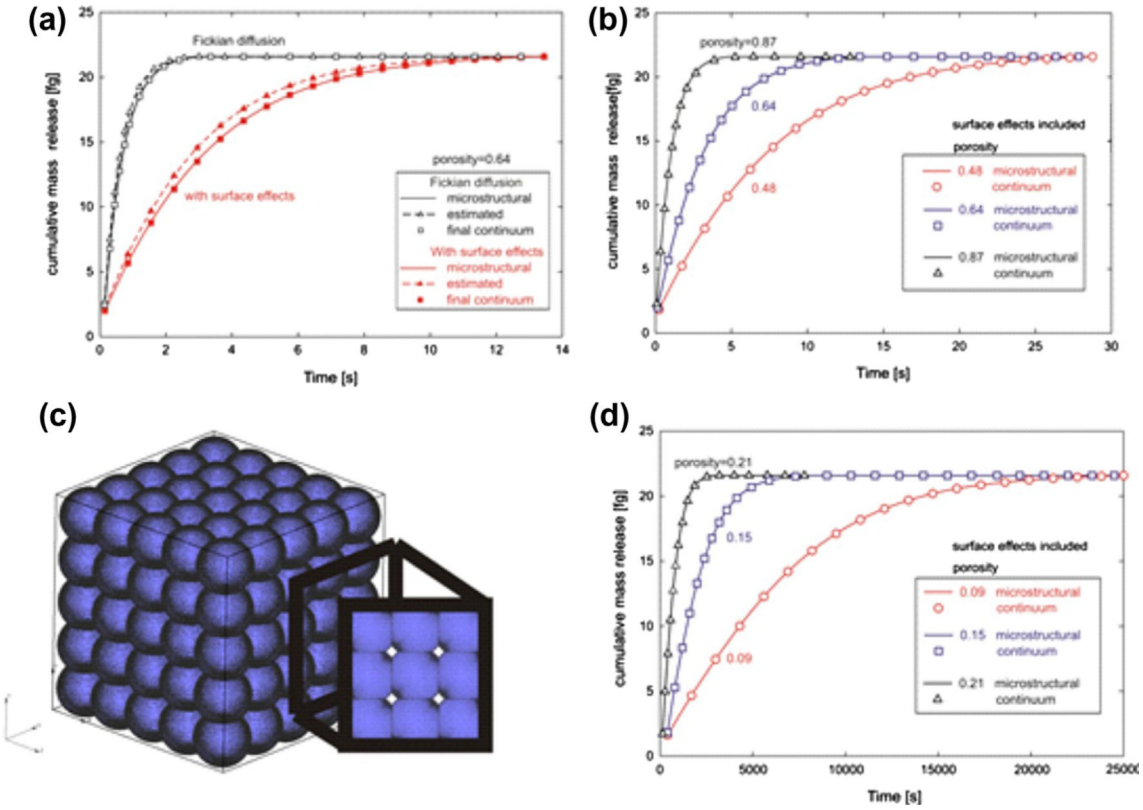

Fig. 10.

Mass release curves for microstructural and continuum models. (a) Diffusion conditions are as described in the caption of Fig. 7. Fickian and surface-affected diffusions are included. Initial continuum mass release curves are calculated using estimated constitutive parameters for the equivalent diffusion coefficient and equivalent distance from surface, and matching of the final continuum solutions (after several iterations from the initial, estimated values) with the microstructural results is achieved; (b) Microstructural and final continuum mass release curves, with surface effects included, for three porosities, for the case when the silica nanospheres are separated as in Fig. 7a; (c) Microstructure consisting of intersecting silica nanospheres; porosity is 9%; (d) Mass release curves for model with intersecting spheres and for three small porosities (9%, 15%, 21%); the time scale is three orders-of-magnitude greater than in Fig. 10b.

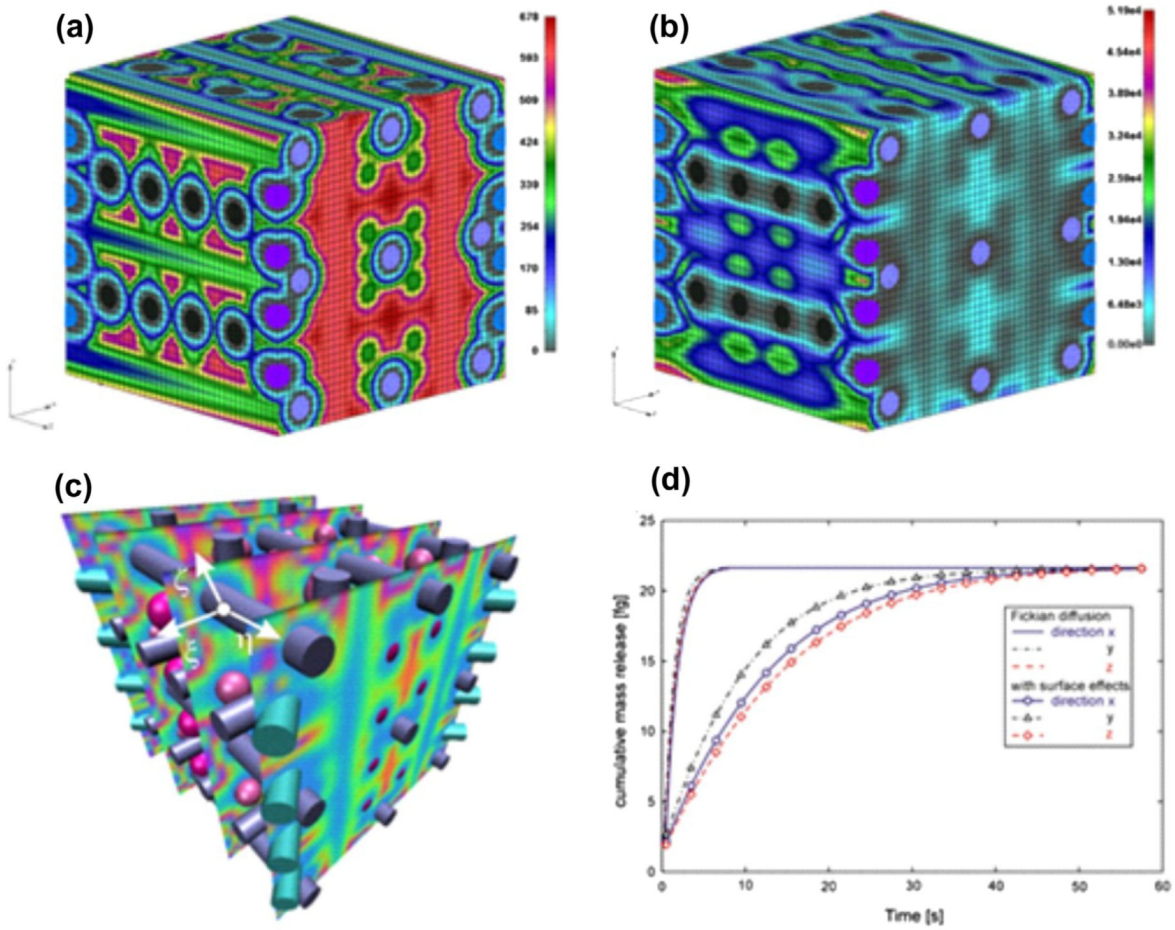

Fig. 11.

Diffusion through a medium with the complex microstructure. (a) Distribution of the x-direction diffusion coefficient D_x on the RV surface at time t = 0.4 s; values span from D_x = 0 (at the solid surfaces and within the solid) to D_x = 678 $\mu m^2 s$.Finite element mesh is shown, porosity is 65%; (b) Distribution of the x-direction flux J_x, displaying a similar character as D_x; (c) Distribution of J_x over several parallel planes. The local coordinate system ξ, η, ζ is shown for a point at the fiber surface. (d) Mass release curves for *x*, *y*, *z* directions, solutions obtained using microstructural and continuum models. Scaling functions for all solid constituents are taken to be the same (shown in Fig. 7b). Equivalent diffusion coefficients are ($\mu m^2/s$): D_x = 148.2, D_y = 201.4, D_z = 164:6, and the equivalent distances are (nm): h_z = 0.53. Although the smallest diffusion coefficient is in the x-direction (hence, mass release kinetics should be the slowest), the slowest mass release is in z-direction since the equivalent distance $h_z < h_x$.

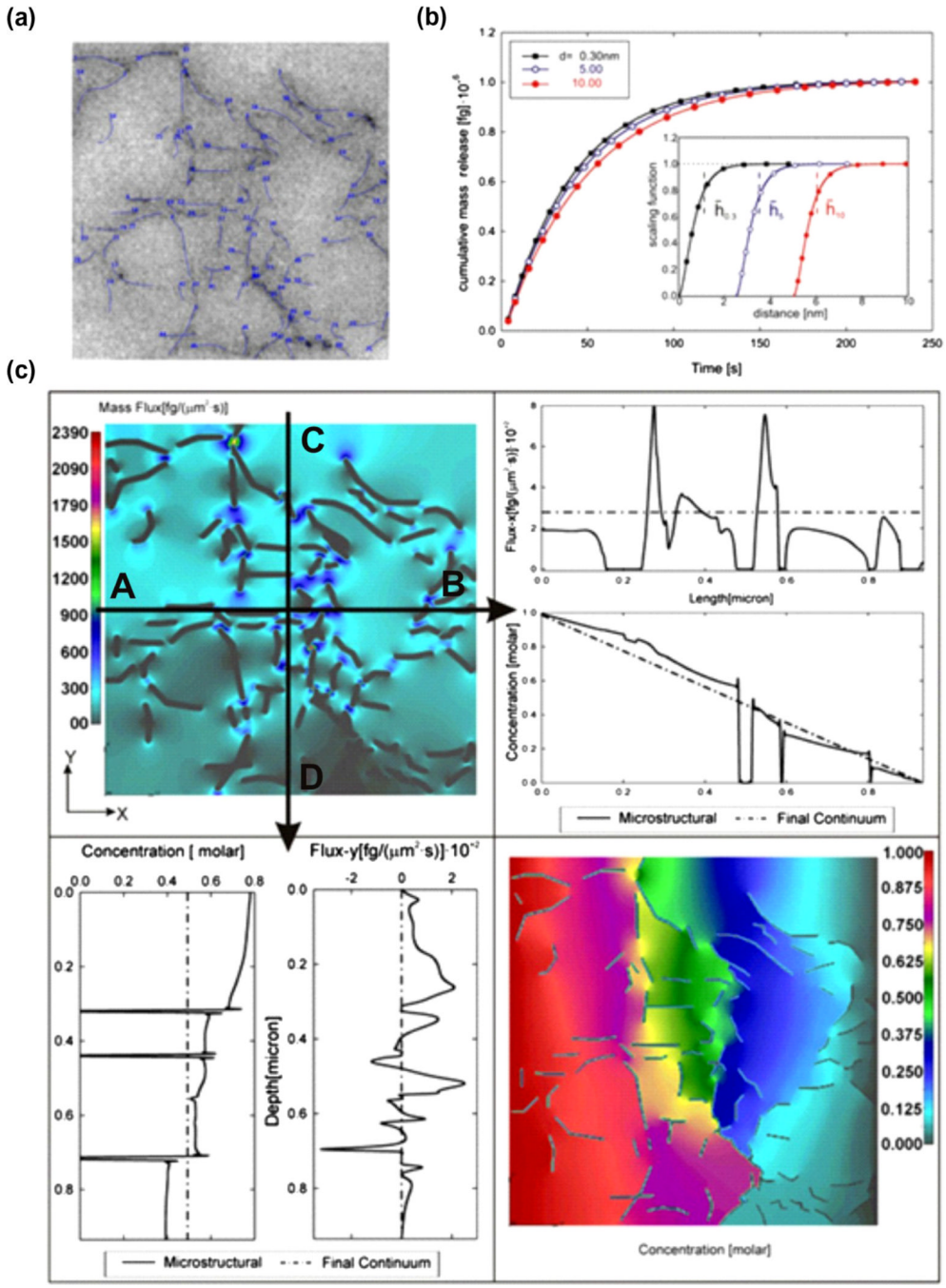

Fig. 12.

Diffusion within an agarose polymeric solution. (a) Internal microstructure obtained by TEM imaging [43] with discretized fibers. The bulk diffusion coefficient is considered independent of concentration, D_{bulk} = 286 μm^2/s. The equivalent diffusion coefficients (in μm^2/s) are: 274, 261, 250 and equivalent distances from surface (in nm) are: 1.12, 3.49, and 6.06 for particle diameters 0.3, 5 and 10 nm, respectively. (b) Mass release curves for three particle diameters 0.3 (rhodamine 6G), 5 and 10 nm. Solutions are the same for microstructural and continuum models. The inset shows the scaling functions for the three particles (displaced to the right for increasing particle radius). (c) Results shown in this

figure are for particle size of 5 nm. Upper left panel: Mass flux-x distribution at time $t = 0.5$ s; dark contours within the field show zero-flux at fiber points. **Upper right panel:** Distribution of mass flux and concentration in the x-direction, microstructural (solid line) and continuum (dashed line) solutions along line A–B; zero-values of flux and concentration correspond to fibers. Continuum model solutions show approximately constant flux-x and linear decrease of concentration along A–B line. **Lower left panel:** Distribution of *y*-direction mass flux and concentration, microstructural (full line) and continuum (dashed line) solution along line C–D; zero-values of flux and concentration correspond to fibers. Continuum model shows constant concentration along B–C line, while mass flux is equal to zero, since there is no diffusion through lateral (*y*-direction) boundaries of the RV. **Lower right panel:** Distribution of concentration at time $t = 0.5$ s, microstructural model; concentration decreases along the x-axis, while zero-values correspond to fibers.

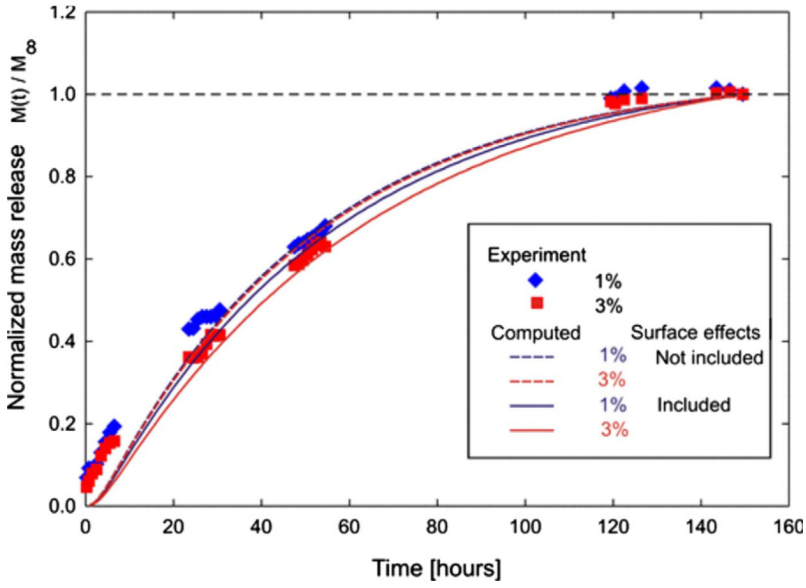

Fig. 13.

Diffusion of rhodamine 6G from reservoir into a sink through a 3 mm thick 1% and 3% agarose hydrogel. Computed (*dashed curves* – without surface effects, *solid curves* – surface effects included) and experiment (*symbols*) data are normalized by maximum released mass M_{∞}.

Table 1

Material parameters D and h for four reservoir volumes V_{in}, with the same initial concentration $c_0 = 2.75$ M/L.

	V_{in} [μL]	D [μm²/s]	h [nm]
1	$7.850 \cdot 10^{-8}$	381.010	0.89676
2	$1.570 \cdot 10^{-8}$	381.010	0.89676
3	$7.850 \cdot 10^{-9}$	381.010	0.90579
4	$1.570 \cdot 10^{-9}$	381.010	0.89676

Table 2

Material parameters D and h for four initial inlet concentrations c_0, and constant reservoir volume $V_{in} = 7.850 \times 10^{-9}$ μL.

	c_0 [M/L]	D [μm²/s]	h [nm]
1	2.75	381.010	0.90579
2	1.75	381.010	0.89133
3	0.75	381.010	0.88764
4	0.01	381.010	0.88455

Table 3

Material parameters $\bar{D}$ and $\bar{h}$ for two sizes of the RV (c_0 = 2.75 M/L).

	a [μm]	$\bar{D}$ [μm^2/s]	$\bar{h}$ [μm]
1	0.04	381.010	0.90579
2	0.08	381.837	0.90128